Superradiance transition in one-dimensional nanostructures: An effective non-Hermitian Hamiltonian formalism

G. L. Celardo and L. Kaplan
Department of Physics, Tulane University, New Orleans, Louisiana 70118, USA
(Received 30 December 2008; revised manuscript received 2 March 2009; published 14 April 2009)

Using an energy-independent non-Hermitian Hamiltonian approach to open systems, we fully describe transport through a sequence of potential barriers as external barriers are varied. Analyzing the complex eigenvalues of the non-Hermitian Hamiltonian model, a transition to a superradiant regime is shown to occur. Transport properties undergo a strong change at the superradiance transition, where the transmission is maximized and a drastic change in the structure of resonances is demonstrated. Finally, we analyze the effect of the superradiance transition in the Anderson localized regime.

DOI: 10.1103/PhysRevB.79.155108 PACS number(s): 72.15.Rn, 73.23.−b, 73.21.Cd, 72.10.−d

I. INTRODUCTION

Open quantum systems are at the center of many research fields in physics today ranging from quantum computing to transport in nanoscale and mesoscopic systems. In particular, electronic transport in the quantum regime can be considered one of the central subjects in modern solid-state physics.[1,2] Transport properties depend strongly on the degree of openness of the system. In important applications, the effect of the opening is large and cannot be treated perturbatively. Thus, a consistent way to take the effect of the opening into account for arbitrary coupling strength between the system and the outside world is highly desirable. The effective non-Hermitian Hamiltonian approach to open quantum systems has been shown to be a very effective tool in addressing this issue.[3–8]

In a typical situation, we have a discrete quantum system coupled to an external environment characterized by a continuum of states. Elimination of the continuum leads to an effective non-Hermitian Hamiltonian.[3–7] Analysis of the complex eigenvalues of the effective Hamiltonian reveals a general phenomenon, namely, the segregation of decay widths (corresponding to the imaginary parts of the complex eigenvalues). Specifically, in a system weakly coupled to the external world, all states tend to be similarly affected by the opening, but once the coupling reaches a critical value, a sharp reconstitution of the system occurs: almost the entire decay width is shared by a few short-lived states, leaving all other (long-lived) states effectively decoupled from the external world. The analogy between decay width segregation and Dicke superradiance[9] has been pointed out in Refs. 4 and 5, although Dicke superradiance is associated with many-body systems, while width segregation occurs also in the one-body case. We will refer to this phenomenon as the "superradiance transition" in the following. Recently, great attention has been given to translating typical quantum optics effects, such as Dicke superradiance, into a solid state context.[10] In particular, the superradiance effect has been shown to occur in several mesoscopic systems.[11]

The effective non-Hermitian Hamiltonian approach to open systems has been used mainly under the assumptions of random matrix theory.[12,13] More realistic systems have also been studied, such as nuclei,[14] electron waveguides,[15] and billiards.[16] In the last example, segregation of resonance widths has already been demonstrated experimentally.[17] The effective non-Hermitian Hamiltonian technique has also been applied to phenomenological open tight-binding models in solid-state physics.[5,18] In these papers, the existence of a superradiance transition in such models was shown, but explicit connections to realistic systems were not considered. For instance, one might ask whether in a realistic situation the coupling to the external environment can be increased up to the point where a superradiance transition occurs. Also, the energy dependence of the effective Hamiltonian is not easy to treat exactly, so one might ask in which realistic applications this energy dependence can be neglected.

In this paper, we consider the problem of transport through a sequence of potential barriers, see Fig. 1, which can be considered a paradigmatic model in solid-state physics. This potential profile appears in real applications, such as semiconductor superlattices or one-dimensional arrays of quantum dots, and has been widely discussed in the literature.[19–21]

The case of equally spaced potential barriers has been analyzed previously.[19] Here a different and more general approach to the problem is considered. First, we show that for weak tunneling coupling among the wells, an *energy-independent* effective Hamiltonian approach produces excellent agreement with an exact (numerical) treatment of the problem. Moreover, it is shown that even in this simple system a superradiance transition occurs as the coupling to the external world is increased by decreasing the widths of the

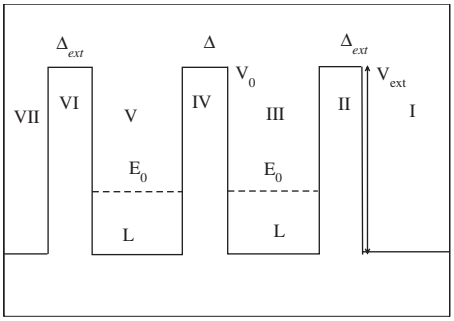

FIG. 1. Sequence of potential barriers of finite height and width.

external potential barriers. With the aid of the effective Hamiltonian approach, we recover several previous results and shed light on the essential features of this well-studied model, allowing for a detailed understanding of the resonance structure. We emphasize that the powerful effective Hamiltonian formalism is not in any way limited to simple models of this type, and can be applied to situations where exact treatment is difficult or impossible. In order to show this, we also analyze the case of random spacings among the potential barriers, and observe the consequences of the superradiance transition in the Anderson localization regime.

After briefly reviewing the effective Hamiltonian formalism in Sec. II, we build the effective Hamiltonian model for a sequence of potential barriers in Sec. III. In Sec. IV, the critical coupling value at which the superradiance transition occurs is derived, and in Sec. V we discuss the consequences of this transition on the resonance structure. In Sec. VI, we show that the maximum transmission is achieved at the superradiance transition, and we estimate analytically the exponential gain in transmission due to the superradiance effect. Finally, in Sec. VII, we consider the superradiance transition in the Anderson localization regime, as a function of the disorder strength.

The effective Hamiltonian approach shows great promise in experimental applications such as quantum dots,[22] photonic crystals,[23] and electron transport in molecular wires.[24] We also believe that the superradiance transition can play a major role in explaining many of the results found in open mesoscopic systems,[22] even if this effect has often been neglected in the literature.

II. EFFECTIVE HAMILTONIAN

We first sketch the essential features of the effective Hamiltonian approach to open quantum systems. Details of the derivation can be found in Refs. 3, 4, 7, and 25.

Consider a discrete quantum system described by N intrinsic basis states $|i\rangle$ coupled to a continuum of states $|c,E\rangle$, where $c=1\ldots M$ is a discrete quantum number labeling M channels and E is a continuum quantum number representing the energy. Let $A_i^c(E)$ be the transition amplitude between the intrinsic states and the continuum. Then the effective Hamiltonian for the intrinsic system, which fully takes into account its opening to the outside, can be written as

$$H_{\text{eff}}(E) = H + P(E) - \frac{i}{2}W(E), \tag{1}$$

with

$$W_{ij}(E) = 2\pi \sum_{c(\text{open})} A_i^c(E) A_j^c(E)^*, \tag{2}$$

where the sum is limited to the open channels, and

$$P_{ij}(E) = \sum_c \text{P.V.} \int dE' \frac{A_i^c(E') A_j^c(E')^*}{E - E'}. \tag{3}$$

Assuming $W_{ij}(E)$ and $P_{ij}(E)$ are smooth functions of the energy, their energy dependence can be neglected if the region of interest is concentrated in a small energy window. With the aid of the effective Hamiltonian, the transmission $T^{ab}(E)$ from channel a to channel b can be determined:

$$T^{ab}(E) = |Z^{ab}(E)|^2, \tag{4}$$

where

$$Z^{ab}(E) = \sum_{i,j=1}^{N} A_i^a \frac{1}{E - (H_{\text{eff}})_{ij}} (A_j^b)^* \tag{5}$$

is the transmission amplitude.

We can also write $T^{ab}(E)$ in a different way, diagonalizing the effective non-Hermitian Hamiltonian H_{eff}. Its eigenfunctions $|r\rangle$ and $\langle\tilde{r}|$ form a bi-orthogonal complete set,

$$H_{\text{eff}}|r\rangle = \mathcal{E}_r|r\rangle, \quad \langle\tilde{r}|H_{\text{eff}} = \langle\tilde{r}|\mathcal{E}_r^*, \tag{6}$$

and its eigenvalues are complex energies,

$$\mathcal{E}_r = E_r - \frac{i}{2}\Gamma_r, \tag{7}$$

corresponding to resonances centered at E_r with widths Γ_r. The decay amplitudes A_i^a are transformed according to

$$\mathcal{A}_r^a = \sum_i A_i^a \langle i|r\rangle, \quad \tilde{\mathcal{A}}_r^b = \sum_j \langle\tilde{r}|j\rangle A_j^b, \tag{8}$$

and the transition amplitudes are given by

$$Z^{ab}(E) = \sum_{r=1}^{N} \mathcal{A}_r^a \frac{1}{E - \mathcal{E}_r} \tilde{\mathcal{A}}_r^b. \tag{9}$$

The complex eigenvalues $\mathcal{E}$ of H_{eff} coincide with the poles of $Z(E)$. It is clear that the properties of the complex eigenvalues of the effective Hamiltonian are very important for understanding the transport properties of the system.

As the coupling between the intrinsic states and the external continuum is increased, a rearrangement of the widths Γ_r occurs. This rearrangement is usually referred to as the "superradiance" transition.

In order to understand the origin of this transition, we can consider a simplified version of Eq. (1): $H_{\text{eff}}=H_0-\frac{i}{2}\gamma W$, where γ is a parameter that controls the coupling strength with the external world (which now we assume to be of the same order of magnitude for all the intrinsic states), and the basis states $|i\rangle$ are chosen to be the eigenstates of H_0, with eigenvalues E_0^i. For small γ, the first-order complex eigenvalues of H_{eff} are $\mathcal{E}_i=E_0^i-\frac{i}{2}\gamma W_{ii}$. If we consider the opposite limit of large γ, H_0 can be viewed as a perturbation acting on W. Due to the factorized structure evident in Eq. (2), W has only M nonzero eigenvalues for $M<N$. Thus, only M states will have a decay width in the limit of large coupling, while all others will have zero width to first order. Therefore, as the coupling increases, all widths initially increase linearly with γ, but at large couplings only M of the widths continue to increase, while the remaining $N-M$ widths approach zero. This simple example suggests that a transition between these two regimes may take place at a critical value of γ. Roughly, the transition occurs when $\gamma/D\approx 1$,[5,13,26,27] where D is the mean level spacing of H_0. Note that the qualitative criterion $\gamma/D\approx 1$ for the transition to superradiance is valid in the

case of uniform density of states and negligible energy shift; when the density of states is not uniform, the transition to superradiance occurs as a hierarchical process.[26] In the case of a non-negligible energy shift, see the analysis in Sec. IV. From the above discussion it should be clear that the superradiance transition emerges in the non-Hermitian effective Hamiltonian approach as a general phenomenon, depending not on the details of the system, but only on the factorized structure of W.

III. EFFECTIVE HAMILTONIAN FOR A SEQUENCE OF POTENTIAL BARRIERS

Let us consider quantum transport through a sequence of $N+1$ potential barriers, see Fig. 1, of width Δ, height V_0, and interbarrier separation L. The transport properties will be analyzed as we change the external barrier width Δ_{ext} while keeping all the other barriers fixed.

We computed the transmission through this system in a standard way, by matching the wave function and its derivative in every region, see Fig. 1. Writing the wave function in region I as $\psi_{\text{I}}=Be^{ikx}$, with $k=\sqrt{E}$, and in region VII as $\psi_{\text{VII}}=Ae^{ikx}+A'e^{-ikx}$, we obtain the transmission coefficient $T(E)=|B/A|^2$ and the reflection coefficient $R(E)=|A'/A|^2=1-T(E)$. For comparing our numerical simulations with experimental results, we note that we work in $\hbar^2/2m_e=1$ units throughout. Thus, when distances Δ, Δ_{ext}, and L in Fig. 1 are measured in nanometers (the typical scale in semiconductor superlattices), all energies are calculated in units of 0.038 eV. In the following we set $L=2$ and $V_0=1000$.

We will now proceed to build an effective non-Hermitian Hamiltonian to describe the quantum transport through a sequence of potential barriers. A sequence of N potential wells can be thought of as a closed system coupled to the continuum of scattering states through the external barriers. Changing the external barrier widths or heights will change the coupling to the continuum. In the limit of low tunneling coupling among the wells, the usual tight-binding approximation can be used to model the closed system: we define the intrinsic basis states $|i\rangle$ as the bound states in each potential well, corresponding to a certain energy level E_0. Each basis state is coupled to its nearest neighbor by the tunneling coupling Ω. For small coupling we have[28,29]

$$\Omega = 2\alpha|\psi(x_0)|^2 = \frac{2\alpha^2 E_0}{V_0(1+\alpha L/2)}\exp(-\alpha\Delta), \tag{10}$$

where $\alpha=\sqrt{V_0-E_0}$, $k=\sqrt{E_0}$, ψ is a basis wave function localized in a single potential well, and x_0 is a point in the middle of a potential barrier immediately adjacent to that well. Due to the tunneling coupling among the N wells, the eigenenergies of the closed system form a miniband around E_0; see Eq. (15) in Sec. IV.

The outside world is characterized by the scattering states to the left, $|L,E\rangle$, and to the right, $|R,E\rangle$, of the sequence of potential barriers. Due to the coupling to the scattering states, the states $|1\rangle$ and $|N\rangle$ acquire a finite width γ and an energy shift δ, which can be computed following Refs. 29 and 30. In the case of a varying external barrier width Δ_{ext}, one obtains

$$\gamma = \frac{8\alpha^3 E_0 k}{V_0^2(1+\alpha L/2)}\exp(-2\alpha\Delta_{\text{ext}}),$$

$$\delta = \frac{k^2-\alpha^2}{4\alpha k}\gamma. \tag{11}$$

Note that the shift δ vanishes for $E_0=V_0/2$; otherwise the sign of δ is given by the sign of $E_0-V_0/2$.

Analogous expressions when the external potential height V_{ext} is varied can be computed by extending the methods of Ref. 29 but are more complicated and will not be reported here. We can now write the full effective Hamiltonian for the miniband centered at energy E_0 as

$$H_{\text{eff}} = \begin{pmatrix} E_0+\delta-\frac{i}{2}\gamma & \Omega & 0 & \cdots & 0 \\ \Omega & E_0 & \Omega & \cdots & 0 \\ 0 & \Omega & E_0 & \cdots & 0 \\ \cdots & \cdots & \cdots & \cdots & \cdots \\ 0 & 0 & 0 & \cdots & E_0+\delta-\frac{i}{2}\gamma \end{pmatrix}. \tag{12}$$

Using Eqs. (4) and (5), the transmission through the sequence of potential barriers becomes

$$T(E) = \left|\frac{(\gamma/\Omega)}{\prod_{k=1}^{N}(E-\mathcal{E}_k)/\Omega}\right|^2. \tag{13}$$

From Eq. (13) we see that the spectrum of complex eigenvalues $\mathcal{E}_k=E_k-\frac{i}{2}\Gamma_k$ of H_{eff} determines the transmission through the system. In order to show the range of validity of the effective Hamiltonian model, we compute the normalized integrated transmission:

$$S = \frac{1}{4\Omega}\int_{E_{\min}}^{E_{\max}} T(E)dE, \tag{14}$$

where the interval $[E_{\min},E_{\max}]$ includes the entire miniband centered at E_0.

The predictions of Eq. (13) are now compared with the exact numerical results. The effective Hamiltonian approach is expected to break down for small values of $\alpha\Delta$. In Fig. 2, we plot S vs $\alpha\Delta$ for a system of $N=10$ wells, with $E_0\approx 20$ fixed, so that α remains constant. From the figure we can see that the effective Hamiltonian approximation gives excellent results for $\alpha\Delta\gg 1$. Note also that S is independent of Δ for $\Delta/\Delta_{\text{ext}}=2$ in the weak coupling limit, $\alpha\Delta\gg 1$, as indicated by a dashed line in Fig. 2. This follows from the fact that γ/Ω is independent of Δ when $\Delta/\Delta_{\text{ext}}=2$, see Eqs. (10) and (11). Note that we also compared the results obtained with the effective Hamiltonian approach with available analytical results found in the literature,[19] and found excellent agreement in the regime $\alpha\Delta\gg 1$.

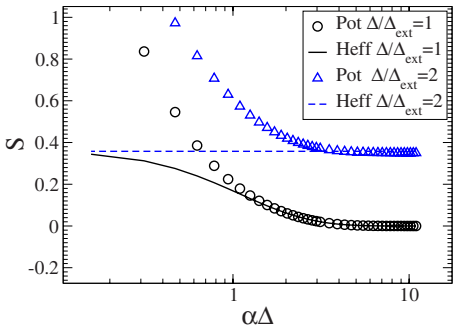

FIG. 2. (Color online) The integrated transmission S is plotted vs $\alpha\Delta$ for a system with $N=10$ wells. Different values of $\alpha\Delta$ are obtained by varying Δ while keeping $E_0 \approx 20$ fixed. The symbols indicate exact numerical results for the sequence of potential barriers, while the lines represent the effective Hamiltonian prediction. The effective Hamiltonian approximation is excellent for $\alpha\Delta \gg 1$. Two values of $\Delta/\Delta_{\text{ext}}$ are shown. The quantities plotted are dimensionless.

IV. SUPERRADIANCE TRANSITION

We will now analyze the superradiance transition that occurs in the effective Hamiltonian model built in Sec. III. Diagonalization of the intrinsic Hamiltonian leads to the energy levels[5]

$$w_q = E_0 - 2\Omega \cos[\pi q/(N+1)], \tag{15}$$

with $q=1\ldots N$. Due to coupling with the external world, the energy levels w_q will acquire decay widths Γ_q. These decay widths are the imaginary parts of the eigenvalues of the effective Hamiltonian, Eq. (12), and, for $\gamma \ll 1$, they can be written as

$$\Gamma_q = \frac{4\gamma}{N+1}\sin^2[\pi q/(N+1)]. \tag{16}$$

We see that all widths increase proportionally to γ for small coupling. In the opposite limit of large γ, only M states (where M is the number of channels) will have a width proportional to γ, while the widths of the remaining states fall off as $1/\gamma$, as explained above in Sec. II. In our case we have $M=2$, corresponding to one scattering channel each on the left and right. The two superradiant states correspond to the two nonzero eigenvalues of the matrix W [Eq. (1)].

In order to find the critical value of the parameter γ at which the superradiance transition occurs, we may analyze the average width $\langle\Gamma\rangle$ of the $N-M$ narrowest widths as a function of the coupling γ, Fig. 3. At the critical value of γ, the average width $\langle\Gamma\rangle$ peaks and begins to decrease. This is the signature of the superradiance transition.

We can evaluate this critical value of γ using the criterion discussed earlier in Sec. II, $\langle\Gamma\rangle/D \approx 1$. Consider first the simpler case of vanishing energy shift δ. The average width $\langle\Gamma\rangle$ is then given by the perturbative expression, Eq. (16), taking into account that $\langle\sin^2[\pi q/(N+1)]\rangle \to 1/2$ for large N. Moreover, from Eq. (15) we find that for large N the mean level spacing becomes $D=4\Omega/N$, so we obtain

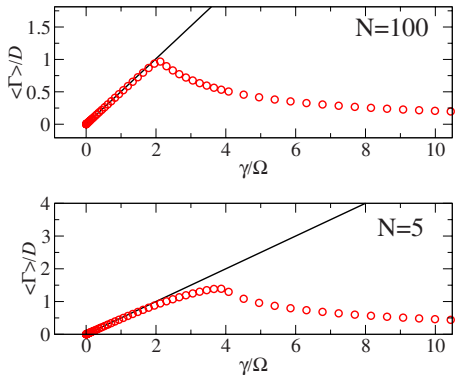

FIG. 3. (Color online) The average width, normalized to the mean level spacing, is shown as a function of γ/Ω for the case $\Delta=0.15$ and $E_0 \approx V_0/2$. When N is large, the transition to superradiance is shown to occur at $\gamma/\Omega \approx 2$, in agreement with the analytical estimation, see text. The solid line corresponds to an average over all N widths, while the symbols are obtained by averaging over the $N-2$ smallest widths. The quantities plotted are dimensionless.

$$\frac{\langle\Gamma\rangle}{D} = \frac{1}{2}\frac{\gamma}{\Omega}. \tag{17}$$

Thus, for $\delta=0$, the criticality criterion $\langle\Gamma\rangle/D \approx 1$ implies $\gamma \approx 2\Omega$. Note that this happens when $\Delta_{\text{ext}}=\Delta/2$ [see Eqs. (10) and (11)], so that the superradiance transition occurs when the external barriers are precisely half as wide as the internal ones.

Typical examples for large and small N are presented in Fig. 3, where $E_0=V_0/2$ to ensure that the energy shift $\delta=0$. The $N=100$ example in the upper panel illustrates that the estimate $\gamma \approx 2\Omega$ for the critical value works very well at large N.

We now turn to the $\delta \neq 0$ case. Both the density of states and the resonance widths are modified, as we can see using second-order perturbation theory in small γ:

$$\mathcal{E}_q = w_q + (\delta - i\gamma/2)\frac{4\sin^2\phi_q}{N+1} + (\delta^2 - \gamma^2/4 - i\gamma\delta)\sum_{p\neq q}\frac{A_{qp}^2}{w_q - w_p}, \tag{18}$$

where $A_{qp}=(2/N)^2[1+(-1)^{q+p}]^2\sin^2\phi_q \sin^2\phi_p$ and $\phi_q = \pi q/(N+1)$.

Clearly, the local level spacings $\Delta_q(\gamma)=\text{Re}(\mathcal{E}_q-\mathcal{E}_{q-1})$ and the local resonance widths $\Gamma_q(\gamma)=-\text{Im}(\mathcal{E}_q+\mathcal{E}_{q-1})$ depend on the index q as well as the coupling γ. A reasonable hypothesis is that the superradiance transition occurs when the resonances begin to overlap locally, i.e., $\Gamma_q(\gamma) \approx D_q(\gamma)$ for some q. We have confirmed numerically that this local overlap criterion gives an excellent approximation for the critical value of γ at which the superradiance transition occurs, for any δ. Unfortunately, second-order perturbation theory does not provide an accurate analytical estimate for γ, confirming that the physics is highly nonperturbative near the superradiance transition.

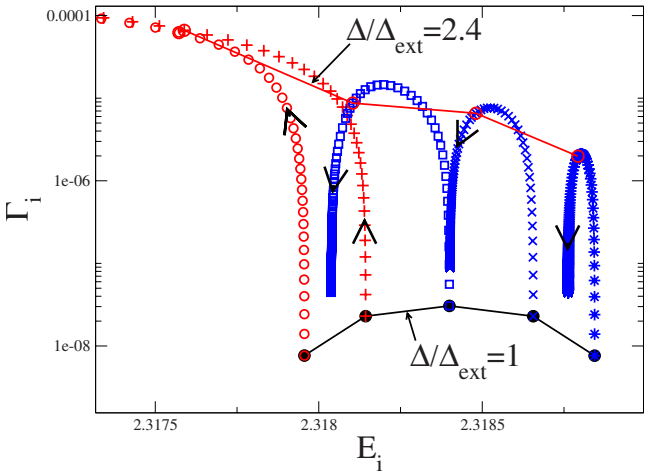

FIG. 4. (Color online) The evolution in the complex plane of the eigenvalues of the effective Hamiltonian is shown as the ratio $\Delta/\Delta_{\text{ext}}$ is varied. A system of five intrinsic states in the $E_0 \approx 2$ miniband is considered, with $\Delta=0.2$. Arrows indicate the motion of the five poles in the complex plane as the width of the external barriers is reduced. The emergence of two superradiant states (circles and crosses) is clearly visible; see the text for further explanation. Here and in the following figures, we use units $\hbar^2/2m_e=1$, so that if lengths Δ, Δ_{ext}, and L are measured in nm, energies are calculated in units of 0.038 eV.

V. RESONANCE STRUCTURE

To show the consequences of the superradiance transition on the transport properties, here we analyze the resonance structure, by considering the transmission $T(E)$. Note that the resonance structure can be directly resolved experimentally; see Ref. 21.

In this section, we focus on the case of $N=5$ potential wells. As discussed above in Sec. IV, a signature of the superradiance transition is the segregation of resonance widths above the critical coupling. The system under study has two open channels, thus we expect two resonance widths (associated with superradiant states) to continue increasing above the transition, while the remaining widths approach zero. In Fig. 4, we show the trajectories of the eigenvalues $\mathcal{E}_i=E_i-i\Gamma_i/2$ of the effective Hamiltonian in the complex plane as $\Delta/\Delta_{\text{ext}}$ is increased. For $\Delta=\Delta_{\text{ext}}$ the positions of the complex eigenvalues are indicated with circles connected by a line near the bottom of the figure. As the external barrier is decreased, the imaginary parts of all eigenvalues initially grow. Above a critical value of Δ_{ext}, the imaginary parts of three complex eigenvalues start to decrease, as indicated by the arrows in Fig. 4, while the imaginary parts of the remaining two eigenvalues continue to increase, as seen in the upper left hand corner of Fig. 4. These are the superradiant states. Note that the real parts of all eigenvalues experience a leftward shift with increasing coupling, since in this case $E_0 < V_0/2$, so that $\delta<0$.

In Fig. 5, the transmission is shown as a function of the energy for several values of $\Delta/\Delta_{\text{ext}}$. For relatively weak coupling, $\Delta/\Delta_{\text{ext}}=1.5$, we have $N=5$ narrow resonances as expected. As we decrease the external barrier widths, the transmission increases and near $\Delta/\Delta_{\text{ext}}=2$ two of the resonances

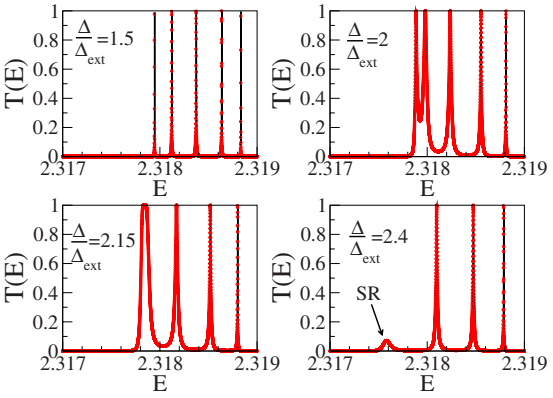

FIG. 5. (Color online) The transmission is shown as a function of energy for a system of $N=5$ potential wells, for the same parameters as in Fig. 4, and several values of $\Delta/\Delta_{\text{ext}}$. The exact transmission, black solid line, is compared with the result obtained from the effective Hamiltonian model, Eq. (13), indicated by red circles. The two superradiant states merge at $\Delta/\Delta_{\text{ext}}=2.15$, and then disappear entirely, leaving behind $N-2$ resonances, see $\Delta/\Delta_{\text{ext}}=2.4$.

start to overlap. The separation between these two resonances and the three remaining ones is due to the nonzero energy shift δ. At $\Delta/\Delta_{\text{ext}}=2.15$, the two overlapping resonances merge, forming one broad resonance. This shows that the superradiance transition has a clear signature in the resonance structure. As the external barrier widths continue to shrink, the height and area of the superradiant resonance peak decrease (see the case $\Delta/\Delta_{\text{ext}}=2.4$ in Fig. 5), until this peak disappears entirely for large $\Delta/\Delta_{\text{ext}}$, due to destructive interference between the two superradiant states. In this limit, $N-2$ narrow resonances remain. The disappearance of the two resonances at very large coupling is not surprising; indeed in the complete absence of the two external barriers, we simply have a system of $N-2$ wells. The interference between the two superradiant states remains destructive if asymmetric couplings to the left and right leads are considered. (Of course, the interference need not be destructive in other geometries; for example in the case of parallel rather than serial coupling to the two leads, the superradiant resonances do not disappear in the limit of strong coupling.)

What is interesting is that the two individual resonances disappear long before the external barriers vanish; indeed they do so immediately after the superradiance transition. Note also in Fig. 5 that results obtained from the effective Hamiltonian model are indistinguishable from numerical results obtained by matching the wave functions.

The behavior we have demonstrated for the case of $N=5$ potential wells generalizes easily to a larger number of wells, with important quantitative differences. Indeed, for a longer chain, the superradiant states disappear much faster as we increase $\Delta/\Delta_{\text{ext}}$ above the critical value, i.e., the superradiance transition becomes increasingly sharp. Interestingly, the critical value of $\Delta/\Delta_{\text{ext}}$ becomes both N independent and E_0 independent in the large-N limit, with the transition occurring at $\Delta/\Delta_{\text{ext}}=2$, in agreement with previous results.[19,21]

VI. INTEGRATED TRANSMISSION

Another interesting quantity to analyze is the integrated transmission S, Eq. (14), as a function of $\Delta/\Delta_{\text{ext}}$. The quan-

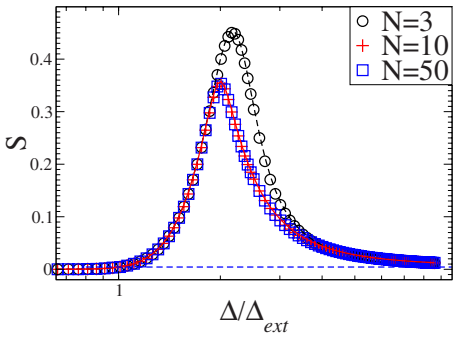

FIG. 6. (Color online) The integrated transmission S is shown as a function of $\Delta/\Delta_{\text{ext}}$, for different numbers of wells. The symbols refer to an exact numerical calculation, while the effective Hamiltonian result for $N=3$ and $N=10$ is indicated by the curves. The horizontal dashed line represents the value of S for $\Delta=\Delta_{\text{ext}}$. In this example, we use $E_0 \approx 20$ and $\Delta=0.15$.

titative enhancement in S when external barrier parameters are adjusted is important in applications, for instance in the design of electron band-pass filters for semiconductor superlattices.[19] From Fig. 6, we see that S reaches a maximum as a function of the external barrier width. Figure 6 also shows that the value of S for $\Delta_{\text{ext}} \ll \Delta$ is the same as for $\Delta_{\text{ext}}=\Delta$. This is due to the fact that S becomes N independent for large N, as shown in Fig. 6: as the external barriers disappear we are eventually left with a sequence of $N-2$ potential wells, which has the same value of the integrated transmission S as the original sequence of N wells.

The maximum of the integrated transmission can be related to the superradiance transition. In Fig. 7, we show the critical value of γ/Ω at which the average width $\langle\Gamma\rangle$ has a maximum (signaling the superradiance transition, see Fig. 3), compared with the value of γ/Ω at which the transmission S has a maximum. For large N, the transmission maximum is reached precisely at the superradiance transition, while for finite N, the specific structure of the resonances influences the exact position of the maximum. The relationship between the superradiance transition and the transmission maximum can be explained as follows: for small γ, the resonance

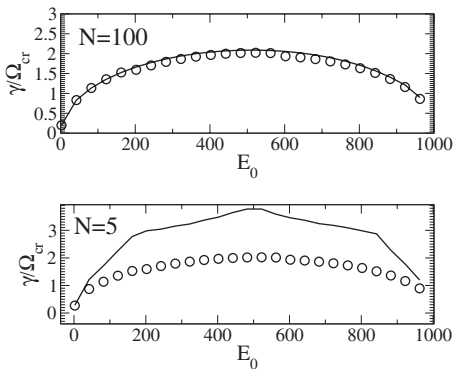

FIG. 7. The critical value of γ/Ω at which the superradiance transition occurs (solid curve) is compared with the critical value at which the integrated transmission has a maximum (circles). For $N=100$ (upper panel), the two coincide, while they differ for $N=5$ (lower panel); see the discussion in the text. Here $\Delta=0.2$.

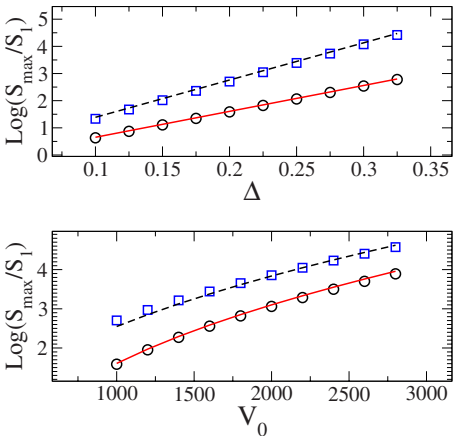

FIG. 8. (Color online) The transmission gain $S_{\max}/S_1$ is shown as a function of the internal barrier width Δ (upper panel) and as a function of the internal barrier height V_0 (lower panel). In each panel, numerical results obtained for energy $E_0 \approx 500$ (circles) and $E_0 \approx 2$ (squares) are compared with the analytical formula (20) indicated by the curves. In the upper panel, we fix $V_0=1000$, while in the lower panel we fix $\Delta=0.2$. All data points are for a system of $N=10$ wells. The numerical prefactor in the analytical result, Eq. (20), is chosen to fit the numerical data.

widths increase with γ, and so does the integrated transmission S. Once the superradiant states start to form, they interfere destructively and the associated resonances disappear, while the widths of the other resonances decrease with γ, leading to an overall falloff in S.

In order to estimate the transmission "gain," we compute the ratio of the maximum transmission to the transmission at $\Delta/\Delta_{\text{ext}}=1$: $S_{\max}/S_1$. The transmission is given by the area under the resonances, and for isolated resonances we can estimate $S \approx 2N\langle\Gamma\rangle/4\Omega$. Since for small γ, see Eq. (16), we have $\langle\Gamma\rangle=2\gamma/(N+1)$, we can write

$$S = \frac{\gamma}{\Omega}\frac{N}{N+1} \approx \frac{\gamma}{\Omega}, \tag{19}$$

which is N independent for large N as noted above. Taking into account that the superradiance transition occurs at $\gamma=2\Omega$ for $E_0=V_0/2$, the gain can be estimated as

$$\frac{S_{\max}}{S_1} \propto \frac{\Omega}{\gamma_1} = \frac{V_0}{4\alpha\sqrt{E_0}} e^{\alpha\Delta}. \tag{20}$$

In Fig. 8, we show that our estimate works very well. Equation (20) is in agreement with the results obtained in Ref. 19 using a different approach. Note also that the gain is exponential in the internal barrier width Δ.

VII. ANDERSON LOCALIZATION REGIME

In the previous sections we considered an effective Hamiltonian (12) with equal diagonal energies E_0. Here we want to apply the effective Hamiltonian technique to the case of random variations in the diagonal energies: $E_0 \pm \delta E_0$, where δE_0 is a random variable uniformly distributed in $[-W/2, +W/2]$, and W is a disorder parameter. A first analysis of this model can be found in Ref. 31.

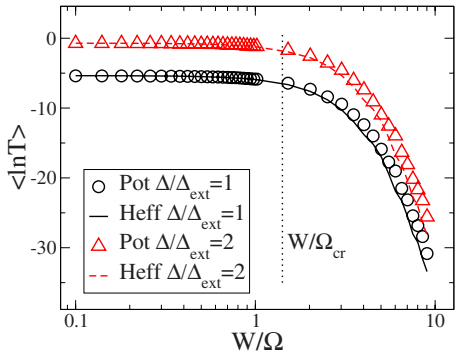

FIG. 9. (Color online) The average of the logarithm of the transmission is plotted as a function of W/Ω for $\Delta/\Delta_{\text{ext}}=1$ and $\Delta/\Delta_{\text{ext}}=2$. Results obtained from the effective Hamiltonian (curves) are compared with results obtained numerically for the sequence of potential barriers (symbols). Here we take $N=50$, $E_0\approx 20$, and $\Delta=0.2$. The dotted vertical line indicates the critical value of W/Ω, obtained from the condition $L_{\text{loc}}=N$, where L_{loc} is given by Eq. (22).

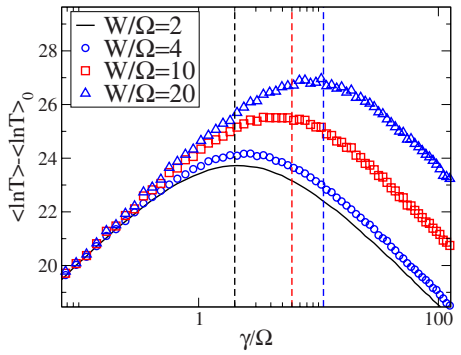

FIG. 10. (Color online) The mean logarithm of the transmission is plotted as a function of γ/Ω, for different values of the disorder parameter W/Ω. Here we take $N=100$, $E_0\approx V_0/2$, and $\Delta=0.6$. The dashed vertical lines indicate the predicted value of γ/Ω at which the transmission maximum is expected for $W/\Omega=2$, 10, and 20, see the discussion in the text. Note that $\langle \ln T\rangle_0$ stands for the value of $\langle \ln T\rangle$ at $\Delta=\Delta_{\text{ext}}$.

Random variation in the diagonal energies can be thought of as a consequence of small random fluctuations δL of the well widths L. For $E_0 \ll V_0$, the eigenenergies of a finite potential well may be approximated by the eigenenergies of an infinite potential well, $E_0=n^2\pi^2/L^2$, where $n=1,2,\ldots$. For small fluctuations $\delta L/L \ll 1$, we have

$$\delta E_0 = \frac{2n^2\pi^2}{L^3}\delta L = -C\,\delta L, \tag{21}$$

where $C=2n^2\pi^2/L^3$. Thus, a random variation of δE_0 in $[-W/2,+W/2]$ corresponds to a random variation of δL in $[-W/2C,+W/2C]$.

The effective non-Hermitian Hamiltonian with diagonal disorder is equivalent to an open Anderson tight-binding model.[2,32] The eigenstates of the Anderson model are exponentially localized on the system sites, with exponential tails given by $\exp(-x/L_{\text{loc}})$, where for weak disorder, the localization length L_{loc} at the center of the energy band can be written as[33]

$$L_{\text{loc}} \approx 105.2\left(\frac{W}{\Omega}\right)^{-2}. \tag{22}$$

For $L_{\text{loc}} \ll N$, the transmission decays exponentially with N; this is the localized regime. Note that for zero disorder, the transmission is N independent, as we showed in the previous section. The condition $L_{\text{loc}}=N$ defines a critical value of $(W/\Omega)_{\text{cr}}$ for the localized regime, at any given N. In the localized regime, the transmission is log-normally distributed, and we have[1]

$$\langle -\ln T\rangle = 2\frac{N}{L_{\text{loc}}} + \text{const.} \tag{23}$$

In Fig. 9, we show the average transmission as a function of the disorder strength for two different degrees of opening of the system. The results obtained using an effective Hamiltonian with diagonal disorder are compared with numerical simulations for the disordered sequence of potential wells. The agreement is excellent up to a large value of the disorder, where of course our approximations break down. [Indeed Ω, Eq. (10), has been computed assuming that the energy levels are aligned, which is no longer true in the presence of disorder.] We stress that Eq. (13) for the transmission remains valid even in the disordered case, making the use of the effective Hamiltonian formalism very efficient, since only the eigenvalues of the effective Hamiltonian are needed to obtain the transmission.

The phenomenon of Anderson localization was studied in a closed disordered chain or for fixed opening, while in our case we can vary the degree of openness of the system. The effect of the opening on Anderson localization is not obvious. Will a maximum of the transmission still exist as we vary the coupling of the system with the external world? Will the localization length change as we open up the system? To answer these questions, we have analyzed the effective Hamiltonian, neglecting the role of the energy shift, i.e., we set $\delta=0$ in the following. In Fig. 10, we compute the average of $\langle \ln T\rangle$ over 10^5 realizations as a function of γ/Ω. The energy is fixed at $E=E_0$. As we vary γ/Ω, the average transmission reaches a maximum, just as in the disorder-free case.

Interestingly, as the disorder strength increases, the transmission maximum (associated with the superradiance transition) shifts to ever higher values of the coupling strength γ. Indeed, the mean level spacing D increases with growing disorder, so that the condition $\langle\Gamma\rangle/D\approx 1$ for the superradiance transition to occur will be satisfied at increasingly larger values of γ/Ω. For weak disorder, the disorder-induced correction to D is second order in the disorder strength, so $(\gamma/\Omega)_{\text{cr}}=2+O(W^2/\Omega^2)$. In the opposite regime of large W/Ω we find $D\approx 2\Omega(1+W/2\Omega)/N$, and the critical coupling is predicted to be $(\gamma/\Omega)_{\text{cr}}\approx 1+W/2\Omega$. This estimate works quite well, as shown by the vertical lines in Fig. 10. Note that the curves shown in Fig. 10 are for $N=100$, but the results have been found to be independent of N.

Finally in Fig. 11, we show $\langle \ln T\rangle$ versus N for $W/\Omega=2$, and for two different values of the external barrier width: $\Delta/\Delta_{\text{ext}}=1$ and $\Delta/\Delta_{\text{ext}}=2$, where the maximum of the transmission occurs. Figure 11 shows that Eq. (23) works very

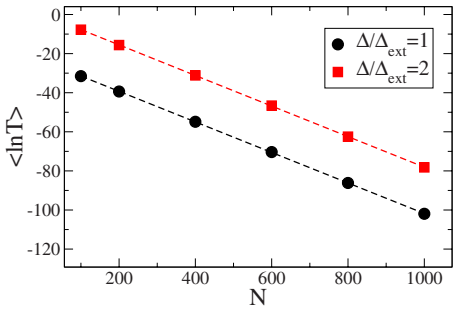

FIG. 11. (Color online) The mean logarithm of the transmission is plotted as a function of N for $\Delta/\Delta_{\text{ext}}=1$ (black circles) and $\Delta/\Delta_{\text{ext}}=2$ (red squares) for the case $W/\Omega=2$, $E_0 \approx V_0/2$, and $\Delta=0.6$. The remaining parameters are the same as in Fig. 9. From the fit we have $\langle \ln T \rangle = a - \nu N$, with $\nu \approx 0.078$, for both $\Delta/\Delta_{\text{ext}}=1,2$, in good agreement with the theoretical result $\nu = 2/L_{\text{loc}} = 0.076$, see Eq. (23).

well in both situations, even though the transmission is enhanced when $\Delta/\Delta_{\text{ext}}=2$, for all values of N. Thus, the localization length in a disordered 1D model is not affected by the opening, but the transmission is.

VIII. CONCLUSION

We have analyzed quantum transport through a finite sequence of potential barriers, a paradigmatic model for transport in solid-state physics. In this paper, the effective non-Hermitian Hamiltonian approach has been used to analyze the transmission through this class of systems. The main results of our work are the following: (i) we show that for weak or moderate tunneling coupling among the potential wells, the system is well described by an energy-independent effective Hamiltonian. Knowledge of the complex eigenvalues of the effective Hamiltonian is sufficient to study transport through the system. Thus the effective Hamiltonian formalism is a simple and powerful tool to analyze quantum transport. (ii) As the coupling to the continuum is increased by adjusting the width of the external barriers, a superradiance transition (or Dicke effect) occurs. Analysis of the complex eigenvalues of the effective Hamiltonian allows us to determine the critical coupling associated with this transition. (iii) The superradiance transition has strong effects on the transport properties: specifically, the transmission through the system is maximized at the superradiance transition. An expression for the transmission gain due to the superradiance transition is derived. Moreover the resonance structure is drastically affected: at the superradiance transition, we have the formation of a broad resonance corresponding to the superradiant states. Beyond the transition, this broad resonance disappears, and the number of resonances decreases by two. (iv) The case of a disordered sequence of potential barriers has been also analyzed. In the presence of disorder, Anderson localization occurs. We have shown the localization length remains constant as the opening changes, but the transmission has a maximum as a function of the coupling to the external world. The critical value of the coupling increases with the degree of disorder, and we obtain an estimate of the critical value for strong and weak disorder, based on the superradiance mechanism. In the future it will be interesting to study the consequences of the superradiance transition beyond the single particle approximation, where electron-electron interactions play an important role.

ACKNOWLEDGMENTS

We acknowledge useful discussions with G. P. Berman, F. Borgonovi, F. Izrailev, S. Sorathia, and V. G. Zelevinsky. G.L.C. is grateful to L. Damiano for fruitful discussions. This work was supported in part by the NSF under Grant No. PHY-0545390.

[1] C. W. J. Beenakker, Rev. Mod. Phys. **69**, 731 (1997).
[2] P. A. Lee and T. V. Ramakrishnan, Rev. Mod. Phys. **57**, 287 (1985).
[3] C. Mahaux and H. A. Weidenmüller, *Shell Model Approach to Nuclear Reactions* (North-Holland, Amsterdam, 1969).
[4] V. V. Sokolov and V. G. Zelevinsky, Nucl. Phys. A **504**, 562 (1989); Phys. Lett. B **202**, 10 (1988).
[5] V. V. Sokolov and V. G. Zelevinsky, Ann. Phys. (N.Y.) **216**, 323 (1992).
[6] I. Rotter, Rep. Prog. Phys. **54**, 635 (1991).
[7] F. M. Dittes, Phys. Rep. **339**, 215 (2000).
[8] A. Amir, Y. Oreg, and Y. Imry, Phys. Rev. A **77**, 050101(R) (2008).
[9] R. H. Dicke, Phys. Rev. **93**, 99 (1954).
[10] T. Brandes, Phys. Rep. **408**, 315 (2005); T. V. Shahbazyan and S. E. Ulloa, Phys. Rev. B **57**, 6642 (1998); T. Vorrath and T. Brandes, *ibid.* **68**, 035309 (2003).
[11] T. V. Shahbazyan and M. E. Raikh, Phys. Rev. B **49**, 17123 (1994); B. Wunsch and A. Chudnovskiy, *ibid.* **68**, 245317 (2003).
[12] J. J. M. Verbaarschot, H. A. Weidenmüller, and M. R. Zirnbauer, Phys. Rep. **129**, 367 (1985); N. Lehmann, D. Saher, V. V. Sokolov, and H.-J. Sommers, Nucl. Phys. A **582**, 223 (1995); Y. V. Fyodorov and H.-J. Sommers, J. Math. Phys. **38**, 1918 (1997); H.-J. Sommers, Y. V. Fyodorov, and M. Titov, J. Phys. A **32**, L77 (1999).
[13] G. L. Celardo, F. M. Izrailev, V. G. Zelevinsky, and G. P. Berman, Phys. Lett. B **659**, 170 (2008); Phys. Rev. E **76**, 031119 (2007); G. L. Celardo, S. Sorathia, F. M. Izrailev, V. G. Zelevinsky, and G. P. Berman, in *Nuclei and Mesoscopic Physics–WNMP*, edited by P. Danielewicz, P. Piecuch, and V. Zelevinsky, AIP Conf. Proc. No. 995 (AIP, New York, 2008).
[14] A. Volya and V. Zelevinsky, Phys. Rev. C **67**, 054322 (2003); Phys. Rev. Lett. **94**, 052501 (2005); Phys. Rev. C **74**, 064314 (2006).
[15] H. Lee and L. E. Reichl, Phys. Rev. B **77**, 205318 (2008).
[16] H.-J. Stöckmann, E. Persson, Y.-H. Kim, M. Barth, U. Kuhl, and I. Rotter, Phys. Rev. E **65**, 066211 (2002); R. G. Nazmitdinov,

H.-S. Sim, H. Schomerus, and I. Rotter, Phys. Rev. B **66**, 241302(R) (2002).
[17] E. Persson, I. Rotter, H.-J. Stöckmann, and M. Barth, Phys. Rev. Lett. **85**, 2478 (2000).
[18] A. F. Sadreev and I. Rotter, J. Phys. A **36**, 11413 (2003).
[19] G. V. Morozov, D. W. L. Sprung, and J. Martorell, J. Phys. D **35**, 2091 (2002); **35**, 3052 (2002); C. Pacher and E. Gornik, Phys. Rev. B **68**, 155319 (2003).
[20] R. Tsu and L. Esaki, Appl. Phys. Lett. **22**, 562 (1973).
[21] C. Pacher, C. Rauch, G. Strasser, E. Gornik, F. Elsholz, A. Wacker, G. Kießlich, and E. Schöll, Appl. Phys. Lett. **79**, 1486 (2001).
[22] M. L. Ladrón de Guevara, F. Claro, and P. A. Orellana, Phys. Rev. B **67**, 195335 (2003); B. H. Wu, J. C. Cao, and K.-H. Ahn, *ibid.* **72**, 165313 (2005); L. Oroszlány, A. Kormányos, J. Koltai, J. Cserti, and C. J. Lambert, *ibid.* **76**, 045318 (2007).
[23] G. A. Luna-Acosta, H. Schanze, U. Kuhl, and H.-J. Stöckmann, New J. Phys. **10**, 043005 (2008).
[24] A. Nitzan and M. A. Ratner, Science **300**, 1384 (2003); L.-Y. Hsu and B.-Y. Jin, Chem. Phys. **355**, 177 (2009).
[25] A. Volya and V. Zelevinsky, in *Nuclei and Mesoscopic Physics*, edited by V. Zelevinsky, AIP Conf. Proc. No. 777 (AIP, New York, 2005), p. 229.
[26] W. Iskra, I. Rotter, and F.-M. Dittes, Phys. Rev. C **47**, 1086 (1993).
[27] C. Jung, M. Müller, and I. Rotter, Phys. Rev. E **60**, 114 (1999).
[28] L. D. Landau and E. M. Lifshitz, *Quantum Mechanics* (Pergamon, Oxford, 1965).
[29] S. A. Gurvitz and G. Kalbermann, Phys. Rev. Lett. **59**, 262 (1987); S. A. Gurvitz, Phys. Rev. A **38**, 1747 (1988).
[30] M. Razavy, *Quantum Theory of Tunneling* (World Scientific, Singapore, 2003).
[31] V. Zelevinsky and A. Volya, in *Proceedings of the 11th Varenna Conference on Nuclear Reaction Mechanisms*, edited by E. Gadioli (University of Milan Press, Milan, 2006), p. 73.
[32] P. W. Anderson, Phys. Rev. **109**, 1492 (1958).
[33] F. M. Izrailev, S. Ruffo, and L. Tessieri, J. Phys. A **31**, 5263 (1998).